ORIGINAL ARTICLE

CIWEM Chartered Institution of Water and Environmental Management | Journal of Flood Risk Management | WILEY

Experimental and numerical modelling of water waves in sewer networks during sewer/surface flow interaction using a coupled ODE-SWE solver

Sadegh Moodi[1] [ID] | Hossein Mahdizadeh[2] [ID] | James Shucksmith[3] [ID] |
Matteo Rubinato[4] | Mehdi Azhdary Moghaddam[1]

[1]Department of Civil Engineering, University of Sistan and Baluchestan, Zahedan, Iran

[2]Department of Civil Engineering, University of Birjand, Birjand, Iran

[3]Department of Civil and Structural Engineering, University of Sheffield, Sheffield, UK

[4]Centre for Agroecology, Water and Resilience, Coventry University, Coventry, UK

Correspondence
Hossein Mahdizadeh, P.O. Box 97175/615, Birjand, Iran.
Email: hossein.mahdizadeh@birjand.ac.ir

Abstract

Flooding in urban areas is expected to increase its magnitude and frequency in the future. Therefore, there is a strong need to better model sewer–surface flow interactions. Existing numerical methods are commonly based on simplified representations of sewer/surface mass exchange, and mainly validated in steady flow conditions. Current methodologies describing the propagation of transient conditions/waves through interaction nodes are simplified, rely on empirical coefficients and/or lack detailed validation. In this paper, an integrated numerical approach for modelling the propagation of water waves through interaction nodes (e.g., manholes) is presented. In this solution, the shallow water equations are used to simulate the free-surface propagation inside the sewer network, and an ordinary differential equation is employed for modelling flow regimes through pipes and manholes. The model proposed is validated against the well-known STAR-CD modelling software for a number of test cases. Finally, further validation is performed against experimental data describing the evolution of water depth around a manhole in unsteady surcharging conditions.

KEYWORDS

coupled flux wave method, experimental model, manhole, numerical modelling, sewer network, shallow water equations

1 | INTRODUCTION

Modelling interactions between piped drainage networks and surface flows is of primary importance for accurate flood risk assessment and planning in urban areas. Although such interactions (via structures such as manholes and gullies) are highly three-dimensional (3D) and complex, current approaches commonly couple pipe network and surface models via simplified representations of interaction nodes based on weir, orifice or other energy equations to represent the exchange of fluid mass (Lee & An, 2019; Martínez et al., 2021; Martins et al., 2018). Although this approach allows practical implementation of modelling tools at urban scales, it also introduces uncertainties when compared to the detailed 3D representation of interaction nodes (Hong &

Kim, 2011). This includes the reliance on empirical energy loss coefficients, which are difficult to define without site-specific calibration (Dong et al., 2021; Kitsikoudis et al., 2021). In addition, it also neglects the transfer of momentum between surface and sub-surface flows which is likely to be significant in the simulation of unsteady events, such as the propagation of flow waves inside drainage systems as well as sudden sewer surcharge events resulting in surface waves (El Kadi Abderrezzak et al., 2009). The SIPSON model introduced almost two decades ago, considered the interaction of overland and sub-surface flows using the weir/orifice formula for characterising flow exchange between major and minor systems (Djordjević et al., 2005). Successively, other studies have followed a similar surface/sub-surface coupling approach to calculate flow mass exchange through interaction nodes (e.g., Fraga et al., 2017; Leandro et al., 2009; Leandro & Martins, 2016; Rubinato et al., 2017). The weir/orifice equation has become a common tool which provides an acceptable approximation of the mass flow exchange if the weir/orifice discharge coefficients are determined properly (Dong et al., 2021; Rubinato et al., 2017), and is implemented in modelling tools such as SWMM. However, this procedure assumes the junctions as momentum-less elements, and therefore, only evaluates the mass conservation, and lacks detailed validation in unsteady conditions (Kitsikoudis et al., 2021). Alternatively, Borsche and Klar (2014) introduced an ordinary differential equation (ODE) system based on the balance of the total energy in the complete network to solve the hydraulic equations of unsteady flow at a pipe/surface interaction node. The proposed ODE system evaluates the height and discharge of the water inside the manhole over each time step. They linked the two-dimensional shallow water equations (2D SWEs) for the surface flow with one-dimensional (1D) Saint-Venant equations governing the sewer pipe and showed the differences between cases with and without the manhole considerations. They investigated the ability of their model in test cases including a coupled surface/sewer system. However, the method was not experimentally validated, or compared with other numerical methods.

Obtaining detailed data sets of urban flooding events and interaction flows is also an ongoing challenge (de Vitry & Leitão, 2020); hence, the robust validation of interaction modelling is problematic. Some previous studies have conducted highly detailed and time-consuming 3D modelling of interaction nodes which enables the testing/comparison of simplified approaches (Beg et al., 2020; Lopes et al., 2015); however, results obtained by these computations are limited to the range of flow conditions and geometries tested

within them, which are normally simplified and steady state. Physical modelling can be used to provide validation data (Rubinato et al., 2021); however, due to the difficulty of characterising unsteady conditions (Rubinato et al., 2017), most available data sets are based on steady flow cases (e.g., Gómez et al., 2019). For example, Martins et al. (2017) tested an alternate 2D shallow water finite volume (FV) solver to model the floodplain water depths affected by known steady surcharging flow from a manhole and validated the obtained results using experimental data. Results confirmed that the modelling approaches provided a good approximation of water depths and hydraulic jump position in the local vicinity of the manhole; however, in this case, the pipe network (and flow exchange) was not explicitly modelled, and tests were limited to steady flow conditions. More recently, Kitsikoudis et al. (2021) presented a methodology for describing mass exchange between surface and sewer systems, and validated this technique by using experimental mass exchange data from the same experimental facility in unsteady conditions. However, this approach still required the derivation of site-specific empirical coefficients to represent turbulent energy losses and did not consider the time series evolution of water depths in the vicinity of the interaction node in transient conditions.

The aim of this paper is first to develop and test a high-order fully integrated (i.e., pipe and surface) modelling approach for surface/sewer interaction flows able to predict the behaviour of the flow inside the sewer system and create more accurate results compared to the existed simplified finite difference and FV approaches. Moreover, the conservation of mass, momentum and total energy are pursued in the proposed approach, with the aim of developing a technique which can consider transient conditions appropriately. The approach will be validated against both 3D Navier–Stokes simulations as well as experimental data sets describing the time series evolution of water depths around manhole during unsteady surcharge events, thereby testing the ability of the modelling approach to describe the transfer of mass and total energy between surface and pipe flows. To obtain a basic understanding, the problem is initially considered in one dimension. However, it is important to note that the proposed method has the potential to be extended to 2D problems, involving multiple manholes, and addressing real risk problems associated with urban flooding.

The remainder of this paper is structured as follows: in Section 2, the governing equations and 1D SWEs are defined. The wave propagation algorithm and the proposed flux-wave approach are introduced. Then, the ODE solver, which approximates the flow into a manhole, is

expressed, and finally, numerical modelling results of different test cases are presented and compared to that of the STAR-CD software (which is a Navier–Stokes solver with free-surface capability, i.e., uses the VOF method to capture the free-surface level) in Section 3. Finally, in Section 3.4, computational results are compared to experimental data sets (flow depths) obtained from a scale model facility of a sewer pipe linked to a free surface flow under an unsteady sewer surcharge event (Rubinato et al., 2017).

2 | MATERIALS AND METHODS

2.1 | Governing equations

The 1D SWEs can be presented as:

$$\frac{\partial h}{\partial t} + \frac{\partial}{\partial x}(q_x) = \omega, \tag{1a}$$

$$\frac{\partial q_x}{\partial t} + \frac{\partial}{\partial x}\left(\frac{q_x^2}{h} + \frac{1}{2}gh^2\right) = -gh\frac{\partial B}{\partial x} - \frac{\tau_{fx}}{\rho}, \tag{1b}$$

where h is the water depth, B denotes the bathymetry gradients, g is the acceleration due to gravity, t is time, $q_x = hu$ is the discharge per unit width, u is the depth-average velocity in the x-direction, ω is the efflux/influx discharge per unit horizontal area, and finally, τ_{fx} is the bed shear stress in the orthogonal direction which can be calculated by:

$$\tau_{fx} = \frac{1}{2}C_f\rho u|u|, \tag{2}$$

where ρ is the water density and C_f is the bed friction coefficient which can be computed based on Manning's coefficient as $C_f = 2gn_m^2/h^{1/3}$ where n_m is Manning's roughness coefficient. The system of equations provided in Equations (1a) and (1b) can be also presented in the form of conservation laws as:

$$\boldsymbol{U}_t + \boldsymbol{F}(\boldsymbol{U})_x = \boldsymbol{S}(\boldsymbol{U},x) \tag{3}$$

where

$$U = \begin{bmatrix} h \\ q_x \end{bmatrix}, \quad F(U) = \begin{bmatrix} q_x \\ \frac{q_x^2}{h} + \frac{1}{2}gh^2 \end{bmatrix}, S = \begin{bmatrix} \omega \\ -gh\frac{\partial B}{\partial x} - \frac{\tau_{fx}}{\rho} \end{bmatrix}. \tag{4}$$

The associated Jacobian matrix for the above system becomes:

$$\mathbf{F}'(\boldsymbol{U}) = \begin{bmatrix} 0 & 1 \\ gh - u^2 & 2u \end{bmatrix}, \tag{5}$$

and the related eigenvalues for the given Jacobian matrices are:

$$\lambda_1^F = u - \sqrt{gh}, \quad \lambda_2^F = u + \sqrt{gh} \tag{6}$$

The super index 'F' denotes the flux-wave method, and the associated eigenvectors become:

$$\boldsymbol{r}_1^F = \begin{bmatrix} 1 \\ u - \sqrt{gh} \end{bmatrix}, \quad \boldsymbol{r}_2^F = \begin{bmatrix} 1 \\ u + \sqrt{gh} \end{bmatrix} \tag{7}$$

For the solution of the conservation law system given in Equation (4), the wave propagation algorithm defined in the next section is used.

2.2 | The 1D wave propagation algorithm

The wave propagation algorithm is a simple way to re-average the Riemann problem into adjacent grid cells for FV methods and was first introduced by LeVeque (1998, 2002). This algorithm can additionally be used within Godunov-type methods to determine fluxes based on the waves and has been successfully applied for many problems including gas dynamics (Bale et al., 2003), SWEs (George, 2008; Mahdizadeh et al., 2011, 2012), morphodynamic systems (Mahdizadeh & Sharifi, 2019) and water-hammer equations (Mahdizadeh et al., 2018). The 1D wave propagation algorithm can be generally expressed in a second-order accurate form:

$$U_i^{n+1} = U_i^n - \frac{\Delta t}{\Delta x}\left(A^+\Delta U_{i-1/2} + A^-\Delta U_{i+1/2}\right) \tag{8}$$

$$- \frac{\Delta t}{\Delta x}\left(\tilde{F}_{i+1/2} - \tilde{F}_{i-1/2}\right),$$

where $\boldsymbol{U}_i^n$ is the vector of conserved variables or unknowns at time $t = n\Delta t$ for cell $C_i \in [x_{i-1/2}, x_{i+1/2}]$ in the FV method, and $\boldsymbol{U}_i^{n+1}$ is the updated version of the vector of unknowns at the next time step. $A^\pm\Delta\boldsymbol{U}_{i\pm1/2}$ are the left- and right-going fluctuations for the x-directions. The terms $\tilde{\boldsymbol{F}}_{i\pm1/2}$ are flux correction terms employed to achieve second-order accuracies with different choice of limiters (LeVeque, 1998, 2002). If $\tilde{\boldsymbol{F}} = 0$, then the first-order Godunov-type method is obtained. The second-order of accuracy considered in this work uses the

second-order term for the spatial and first-order for the temporal discretisation, which gives more accurate results in particular for the problems containing shock features within the solution. The first-order model is rather diffusive compared to the second-order. The right and left-going fluctuations, $A^{\pm}\Delta U_{i\pm 1/2}$ at each FV cell interface can be computed using the flux-wave formula explained in the next section.

2.3 | Flux-wave formula

To solve the system presented in Equations (1a) and (1b) based on the 1D wave propagation algorithm, the Riemann problem should be solved. Therefore, the conservation law problem $U_t + F(U)_x = S$ is solved using the flux-wave formula to obtain $A^{\pm}\Delta U_{i\pm 1/2}$. The Flux-wave formula was originally introduced by Bale et al. (2003) and can be stated as:

$$F(U_i) - F(U_{i-1}) - S_1\Delta x = \sum_{k=1}^{M_w} \boldsymbol{\xi}_{k,i-1/2}, \quad (9)$$

where $\xi_{k,i-1/2}$ is called the flux-wave, which is calculated by multiplying a constant coefficient $\beta_{k,i-1/2}$ by the eigenvector in the form of Equation (7) $\xi_{k,i-1/2} = \beta_{i-1/2}\boldsymbol{r}^F_{k,i-1/2}$ and M_w shows the number of waves, which for the 1D SWEs is equal to 2. The corresponding fluxes and the source term in the x-direction can be given by:

$$F(U) = \left(q_x, \frac{q_x^2}{h} + \frac{1}{2gh^2}\right)^T, \quad S_1 = \left(\omega_{i-\frac{1}{2}}, ghB_x - \frac{\tau_{fx}}{\rho}\right)^T. \quad (10)$$

To employ the flux-wave formula, first, the differences between fluxes for adjacent FV cells are presented as a vector ΔF:

$$\begin{bmatrix} 1 & 1 \\ s_{1,i-1/2} & s_{2,i-1/2} \end{bmatrix} \begin{bmatrix} \beta_1 \\ \beta_2 \end{bmatrix} = \begin{bmatrix} \Delta F_1 \\ \Delta F_2 \end{bmatrix}, \quad (12)$$

where $s_{1,i-1/2}$ and $s_{2,i-1/2}$ are the first and second wave speeds which are calculated based on the formulae proposed by Mahdizadeh et al. (2011). Solving the linear system in Equation (12) gives the relevant β_1 and β_2 coefficients, which are in turn used to determine $A^{\pm}\Delta U_{i\pm 1/2}$. For more details of calculating the true cross derivatives to obtain fully second-order accurate results, see Mahdizadeh et al. (2012) and LeVeque (2002).

2.4 | Manhole model

In this work, the ODE introduced by Borsche and Klar (2014) is adopted for modelling the height and discharge of water through the manhole:

$$\begin{pmatrix} h_M^j \\ Q_M^j \end{pmatrix}_t = \begin{pmatrix} \dfrac{Q_M^j + Q_{ext}^j}{A_M^j} \\ \dfrac{gA_M^j}{h_M^j}\left(\overline{h}_{node}^j - \overline{h}_M^j\right) - \Delta L_M^j \end{pmatrix}, \quad (13)$$

where h_M represents the water height in the manhole calculated from the sewer invert level and Q_M and Q_{ext} are inflows from the bottom and top, respectively. Additionally, A_M is the cross-sectional area of the manhole, $\bar{h}_M$ is the hydraulic head of the manhole and $\bar{h}_{node}$ is the hydraulic head at junctions. The term ΔL_M summarises energy losses due to friction. This can be represented by the Darcy–Weisbach formula (as in Borsche & Klar, 2014) and hence can be obtained from:

$$\Delta L_M^j = \frac{\lambda_{DW}^j}{8} U_M^j Q_M^j \frac{\left|Q_M^j\right|}{\left(A_M^j\right)^2}, \quad (14)$$

$$\Delta F = \begin{bmatrix} \Delta F_1 \\ \Delta F_2 \end{bmatrix}$$
$$= \begin{bmatrix} q_{x(i)} - q_{x(i-1)} - \Delta x\omega_{i-1/2} \\ \left(\dfrac{q_{x(i)}^2}{h_i} + \dfrac{1}{2}gh_i^2\right) - \left(\dfrac{q_{x(i-1)}^2}{h_{i-1}} + \dfrac{1}{2}gh_{i-1}^2\right) - g\Delta x\left(\dfrac{B_i - B_{i-1}}{2}\right)(h_i - h_{i-1}) + \Delta x\dfrac{\tau_{fx(i)} + \tau_{fx(i-1)}}{2\rho} \end{bmatrix}, \quad (11)$$

where i and $i-1$ are the left and right states of the cell interface $i-1/2$. The vector of ΔF is then equalised to the summation of flux-waves, $\sum_{k=1}^{M_w}\xi_{k,i-1/2}$, terminated to the following system of equations:

where λ_{DW} and U_M are the Darcy–Weisbach coefficient and manhole perimeter, respectively. The fourth-order Runge–Kutta method is used here to solve Equation (13).

2.5 | Coupling surface and sub-surface flow

The most important contribution of this research is the coupling of unsteady surface and sewer network flows via a manhole. The proposed approach, hereafter referred to as the coupled flux wave (CFW) method, utilises the second-order FV method for both free-surface and underground flows. The overland flow is linked to the sub-surface flow using an ODE solver introduced by Borsche and Klar (2014) (Equation 13). Moreover, both inflow and outflow discharges are treated within the continuity equation and are handled within the flux-differencing of the FV neighbouring cells using the flux-wave formula. This preserves the entire solution in agreement with the laws of energy conservation even when the exchange between the surface and the sewer network (and vice versa) is taking place. To achieve this goal, the total energy in the sewer network is conserved utilising this integrated approach. The ODE system proposed by Borsche and Klar (2014) provides the height and discharge within the manhole. Here, water height and the discharge are calculated using the proposed ODE, and then imported to the underground pipe equations at each step. This procedure is mutual, that is, the sign of the calculated discharge determines whether the flow is influx or efflux.

2.6 | Test cases

Four different generalised flow situations are investigated here. Three of these are validated via comparison to a 3D CFD model (STAR-CD), with the final test case validated against experimental data. The first case investigates the interaction of surface flow with surcharged manholes where dam-break flow moves on a surface and interacts with two surcharging manholes. The second situation is related to conditions where the manhole is empty and the inflow is imposed uniformly on the manhole from the surface. Thereafter, the flow is governed by the manhole equations, and after passing through the manhole, reaches the underground sewer pipe as depicted in Figure 1. Here, the underground sewer system is simulated with the proposed 1D shallow water solver. Furthermore, a dimensionless number, called the manhole number (MN), is introduced for this case, and defined based on drop height, manhole size, velocity of input flow and distance between the manholes. The MN is used to define acceptable performance range for the modelling approach.

The third situation takes place when 1D or 2D surface flow exists. In this setting, two water volumes from two
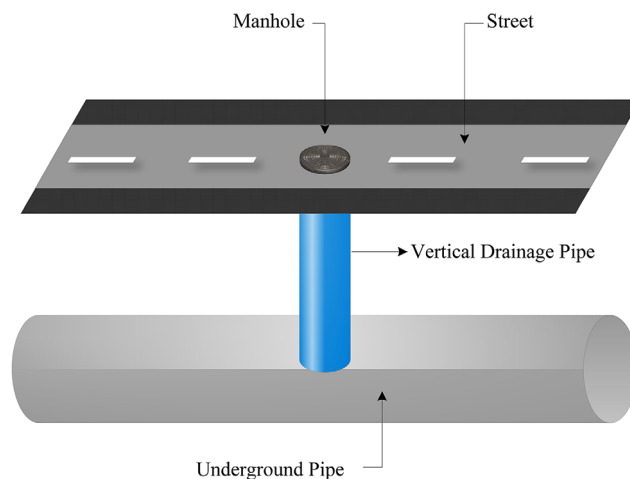

FIGURE 1 Schematic presentation of the linkage via a manhole of an urban street and underground sewer pipe.

opposite directions, and in the form of symmetric dam breaks, start flowing and colliding in the manhole. Then, the flow descends through the manhole shaft and propagates through the pipe network. It is to be noted that SWEs do not have the ability to model a free-fall, and therefore, first, the SWEs are solved for the surface flow (where they exist) to obtain the velocity and discharge at the inlet of the manhole. Then, these values are included in the manhole equations, and the output discharge is used as an entering flow for the SWEs to simulate the sewer network. Finally, experimental data is used to validate the model in the case of time-varying conditions which transition between net flow exchange from the surface to the pipe (influx) and net flow exchange from the pipe to the surface via a manhole. Further details of the experimental facility, measurement techniques and testing conditions are described in Rubinato et al. (2017).

2.7 | STAR-CD software

STAR-CD is a mesh-based commercial software capable of 3D simulating the wide range of physical problems such as free surface flows, multiphase problems, buoyancy, and so on. In this software, the differential equations governing the conservation of mass, momentum, energy, and so on, within fluid and solid systems, are discretised by the FV method (Gosman, 1969; Patankar, 1980). Thus, they are first integrated over the individual computational cells and then approximated in terms of the cell-cantered nodal values of the dependent variables. In addition, STAR-CD employs implicit methods to solve the algebraic FV equations resulting

from the discretisation practices. STAR-CD currently incorporates two implicit algorithms, namely:

- A variant of the well-known SIMPLE method (Patankar & Spalding, 1972; Schmidt et al., 1997).
- The PISO method (Issa, 1986; Issa et al., 1991).

The SIMPLE method is used in this paper. In STAR-CD, only implicit schemes for time advancement are used. This means that diffusive and convective fluxes and source terms are computed only at the current time. Two options for approximating the time derivative are offered. The choice depends on the solution algorithm used. In the case of SIMPLE, the available options are:

- The first-order, fully implicit Euler scheme
- The second-order, fully implicit scheme with three-time levels (also called 'quadratic backward implicit')

As a result of the decoupling of the equation for each dependent variable and subsequent linearisation, large sets of linear algebraic equations are obtained. To solve these equations, STAR-CD uses the following techniques:

- Conjugate gradient (CG)-type solvers with various pre-conditioning methods.
- The algebraic multigrid (AMG) approach which uses the usual multigrid methods of solving matrix equations without relying on the geometry of the problem being solved.

STAR-CD contains built-in boundary condition options that cover the majority of practical situations. In this paper, three boundary conditions, including inlet, pressure and wall, are utilised. The pressure boundary condition is assigned to those parts of the model that are in touch with the atmosphere. The entrances are represented by inlet boundary condition, and the other sides are wall. In addition, the 3D nature of STAR-CD is simplified to a 2D model considering the thickness of the rectangular model as only one cell. Furthermore, this software provides different turbulence models such as k-ε high/low-Reynolds number, k-ω, V2F, LES, and so on. In this paper, the V2F and k-ε high-Reynolds number turbulence models are utilised for the simulation. The particular high Reynolds number form of the k-ε model used in STAR-CD is 'appropriate', subject to the caveats given earlier, to fully turbulent, incompressible or compressible flows (Tahry, 1983). It also allows to some extent for buoyancy effects (Rodi, 1979).

3 | RESULTS AND DISCUSSION

For the first three test cases, the achieved numerical results were compared with those of the 3D Navier–Stokes solver and STAR-CD solver. To better approximate the geometry of the test cases, the thickness of the model in STAR-CD is considered equal to one cell width. By using this approach, the 3D model is converted to a 2D model and therefore it becomes comparable with 1D SWEs. The friction is set equal to $C_f = 0.002$ for all test cases. The CFL number and the number of computational cells were defined separately for each test case. The extrapolation boundary condition has been used by setting U_0 and U_{-1} equal to U_1. The Non-reflecting boundary condition is achieved by this condition (LeVeque, 1998). The in/out-flow is added through the source term in the continuity equation.

3.1 | Dam-break interaction with two surcharging manholes

In this test case, the interaction of dam break flow with two surcharging manhole flows released onto a dry bed is studied. This test case is important as it shows the ability of the proposed CFW method in modelling multiple wave interactions over the dry state. As shown in Figure 2, the left-hand side water volume has dimensions of 2 m width and 0.2 m height. Centres of the manholes are located at $x = 1$ m and $x = 2.6$ m from the end of the initial water volume, and the diameter of the manholes is set to 0.2 m. In addition, the flow surcharges with a uniform 0.1 m/s velocity.

The values are selected similarly to the previous work (Mahdizadeh et al., 2011) to satisfy the Efflux number $EN = V/\sqrt{gl}$ set to $EN = 0.071$ for each opening where in this equation V is the velocity of outflow, l is the manhole diameter and g denotes the acceleration due to gravity. The EN is a dimensionless number defined to better study the behaviour of flow in terms of efflux/influx discharges. It is similar to the Froude number and is determined by dividing the velocity by the square root of the product of gravitational acceleration and a characteristic length (manhole diameter). This formulation captures the relationship between the flow velocity and the geometric characteristics of the system. The EN is involved here to provide a comparison for the reader within previous studies conducted. Figure 3 compares the results of the proposed CFW method with STAR-CD outputs at times 0.4, 0.8, 1.2 and 1.6 s for this test case.

As it can be observed, the interaction between the rarefaction wave created by the dam-break flow and the first outflow happens at time $t = 0.4$ s and the resulting waves move into the second surcharged flow located downstream. At time $t = 1.2$ s, a full interaction of the dam-break flow with both outflows has occurred. Results indicate that the CFW approach agrees closely with the Navier–Stokes results (Figure 3c). Small discrepancies

FIGURE 2 Initial condition for the dam-break interaction problem.
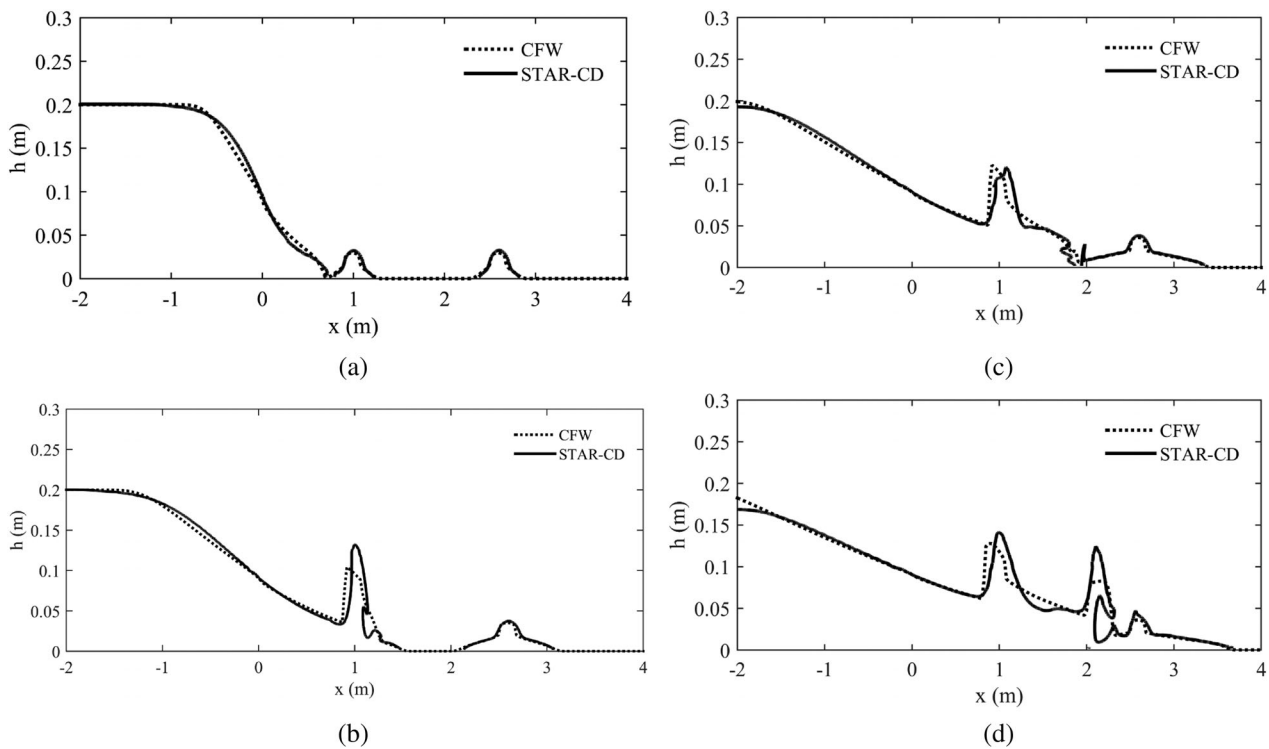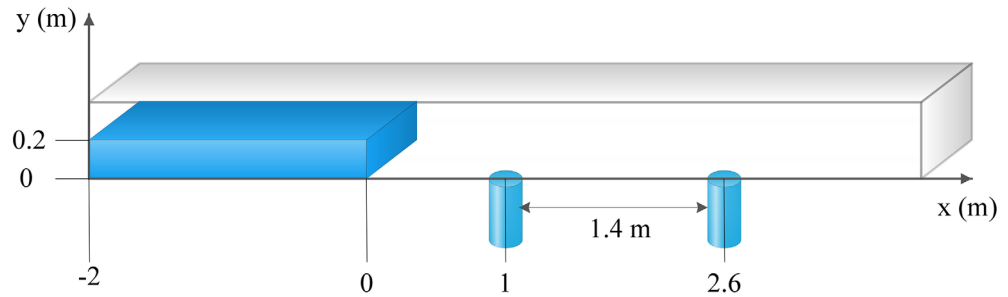

FIGURE 3 Comparison between the solutions of the SWE-based CFW approach and NSE-based STAR-CD for modelling the interaction between the dam break and two surcharged flows at (a) 0.4, (b) 0.8, (c) 1.2 and (d) 1.6 s. CFW, coupled flux wave; NSE, Navier–Stokes equation; SWE, shallow water equation.

(up to 0.1065 m) are observed between the shallow water and STAR-CD results, due to the depth-average nature of the proposed method. For example, the water waves at the moment of collision in STAR-CD results have higher height than CFW results. As time passes, this difference in height becomes less and better agreement between the results can be observed. For the CFW approach, 512 computational cells with Courant number $Cr = 0.5$ are used. The k-ε high-Reynolds number turbulence model is employed in STAR-CD, regarding the fully turbulent flow based on the calculated Reynolds number much greater than 2000. Additionally, a mesh with $dx = 0.005$ is utilised and at the location of collision (from 0.5 to 2.5 m in x-direction and from 0 to 0.15 m in y-direction), the mesh is refined by reducing dx to half of its initial size. To compare the accuracy of the CFW in more detail, the error

norms between the results of the two approaches were calculated using the following equation:

$$l_2 = \frac{\sqrt{\sum (dh_i)^2}}{n}, l_\infty = max(|dh_i|), \quad dh_i = y_{N-S} - y_{SWEs},$$
(15)

where y_{N-S} (m) is the depth of flow in STAR-CD's model, y_{SWEs} (m) is the water depth from the CFW model and n shows the number of comparison points. The error norms for the results shown in Figure 3 are calculated and shown in Table 1 indicating that, in general, a good level of agreement is obtained between the two approaches. The SWEs take 1.14 s, whereas the STAR-CD calculation takes 1330.75 s using the same computer processor and memory.

3.2 | Two manhole system

This section investigates the flow in a sewer network with two inflows, where water enters into a horizontal sewer system through the vertical manhole pipes located at distance equal to 2 m from each other, as illustrated in Figure 4. Each vertical pipe has a length and diameter of 0.3 and 0.1 m, respectively, and a uniform inflow velocity is imposed. After passing through the manholes, the flow enters the sub-surface pipe and propagates on a dry-state bed.

To explore the performance of the CFW considering hydraulic and geometrical conditions, a dimensionless manhole number is defined:

$$MN = \frac{V}{\sqrt{g\frac{lh}{d}}}, \qquad (16)$$

where l is the manhole diameter, h is the length of the manhole plus the underground channel height, d denotes the horizontal distance between manholes and V shows the inflow velocity. The value MN considers the range of conditions under which the shallow water equations may be applied to the efflux/influx problems. The number is a function of the velocity, gap length and manhole height, and may be used to consider the performance of the modelling approach under different characteristic conditions. To investigate different possible cases and examine the performance of the defined number, three different vertical pipe uniform inflow velocities of 0.5, 1 and 1.5 m/s

giving manhole numbers $MN = 1.0098, 2.0196$ and 3.0294 were considered.

Figure 5 compares the simulation results by the CFW and STAR-CD approaches for MN = 1.0098. As can be observed, the width of the water column in STAR-CD results is smaller than the CFW solution. This is due to the small value of water velocity at the inlets. The water at height 0.5 m has the width of 0.1 m, but at the end of the manhole length ($h = 0.2$ m), this width becomes smaller than the manhole width. At time $t = 0.5$ s, the STAR-CD results show that the two inflows have passed through the length of the manholes and spread over the dry bed in the underground channel. The wavefronts show the higher speed in the STAR-CD solution. Due to the VOF = 0.5 capturing, some droplets collide with each other at the centre of the domain. For the later times ($t = 0.9$ s), as evident in Figure 5c,d, a rather obvious discrepancy (0.04 m difference in height at collision point) is observed between the CFW and STAR-CD approaches. However, it is evident that the CFW solver is still able to predict the front waves propagating over dry state within the underground channel. Figure 6 depicts the numerical results for the MN = 2.0196 case. As can be seen, the interaction between the manhole flows occurs at time $t = 0.7$ s in the underground pipe. At time $t = 0.9$ s, the height of water increases at the collision point based on the CFW results, whereas the water volume drops and causes a cavity in the STAR-CD solution. Additionally, for the spaces between the inflows, some small discrepancy is observed in the results of the two methods, which is due to the inability of the CFW solver in modelling the water jet inside the vertical pipe. In general, and compared to the previous case (MN = 1.0098), the simulations of the CFW approach for this manhole number have a much better agreement with the Navier–Stokes solver.

In Figure 7, the numerical results corresponding to MN = 3.0294 are illustrated. As can be observed, the CFW solutions, calculated with the assumption of hydrostatic pressure distribution, are in good agreement with the results of the STAR-CD solver. However, in terms of front waves, both CFW and STAR-CD give near-identical results confirming the effectiveness of CFW in the

TABLE 1 Error norm between the simulation results of SWE and NSE solvers in modelling the interaction of dam break and two-bed flows.

Time (s)	l_∞	l_2
0.8	0.1053	3.0716×10^{-4}
1	0.1065	2.4960×10^{-4}
1.2	0.0982	2.7497×10^{-4}
1.4	0.0925	3.0153×10^{-4}

Abbreviations: NSE, Navier–Stokes equation; SWE, shallow water equation.
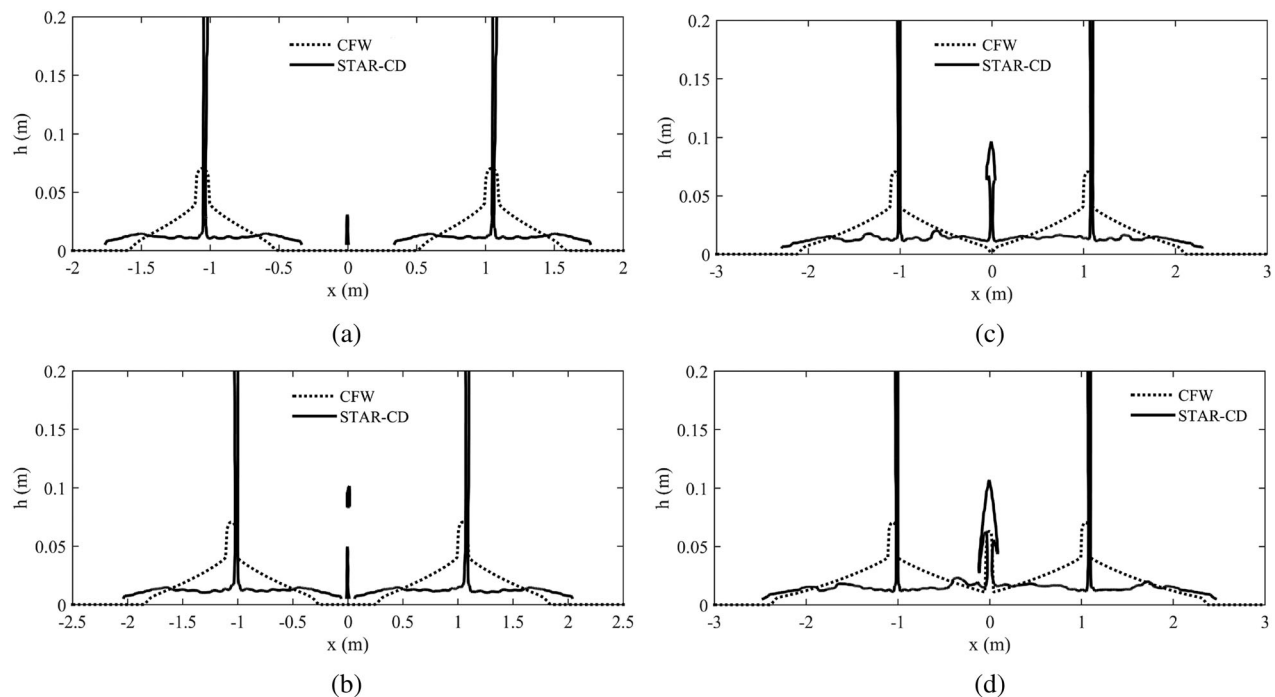

FIGURE 4 Schematics of a sub-surface sewer pipe with two manholes.

FIGURE 5 Comparison between the simulation results of the CFW and STAR-CD approaches in modelling sewer flow with two inflows for MN = 1.0098 at times $t = 0.5, 0.7, 0.9$ and 1.1 s (a–d). CFW, coupled flux wave; MN, manhole number.
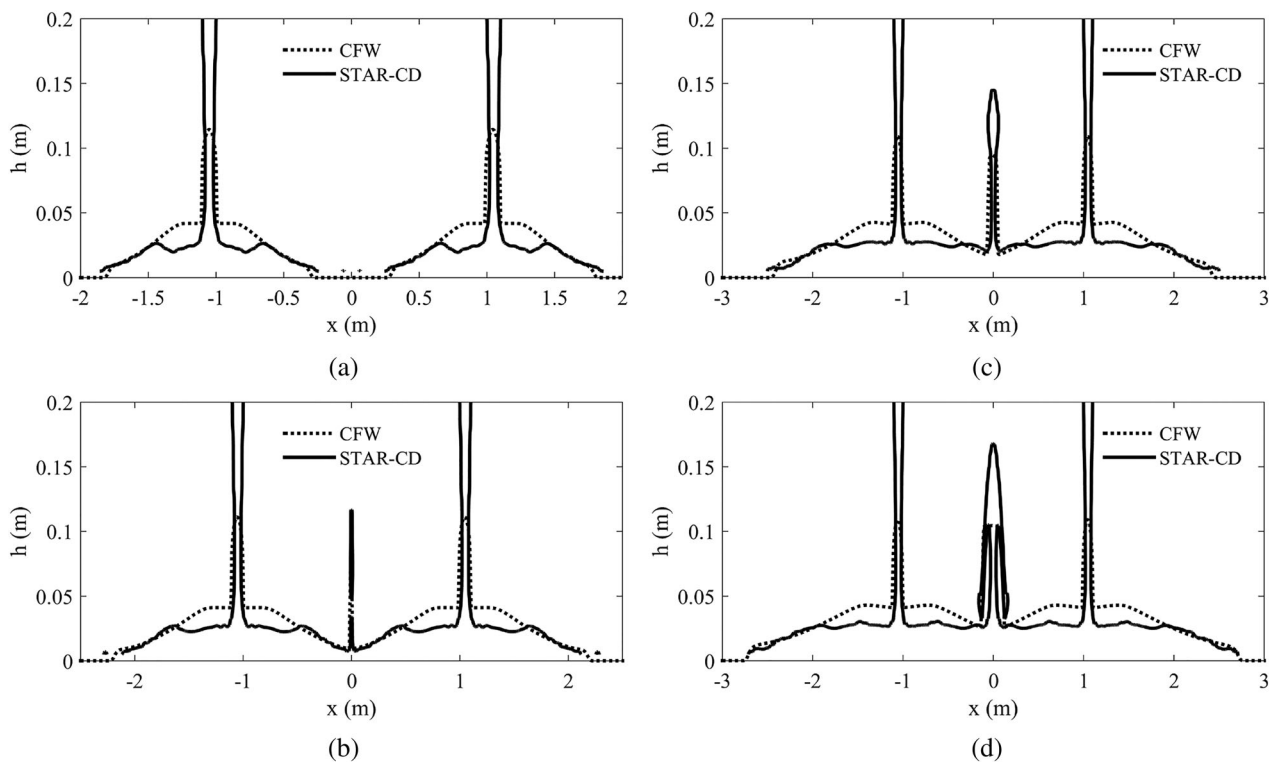

FIGURE 6 Comparison between the simulation results of the CFW and STAR-CD approaches in modelling sewer flow with two inflows for MN = 2.0196 at times $t = 0.5, 0.7, 0.9$ and 1.1 s (a–d). CFW, coupled flux wave; MN, manhole number.

prediction of waterfronts for large manhole numbers. However, the height of water in the pipe network right under the manhole location in the underground pipe, is not identical in two approaches. This is because the CFW is not capable of accurately modelling the falling water through the interaction node. Therefore, the falling flow
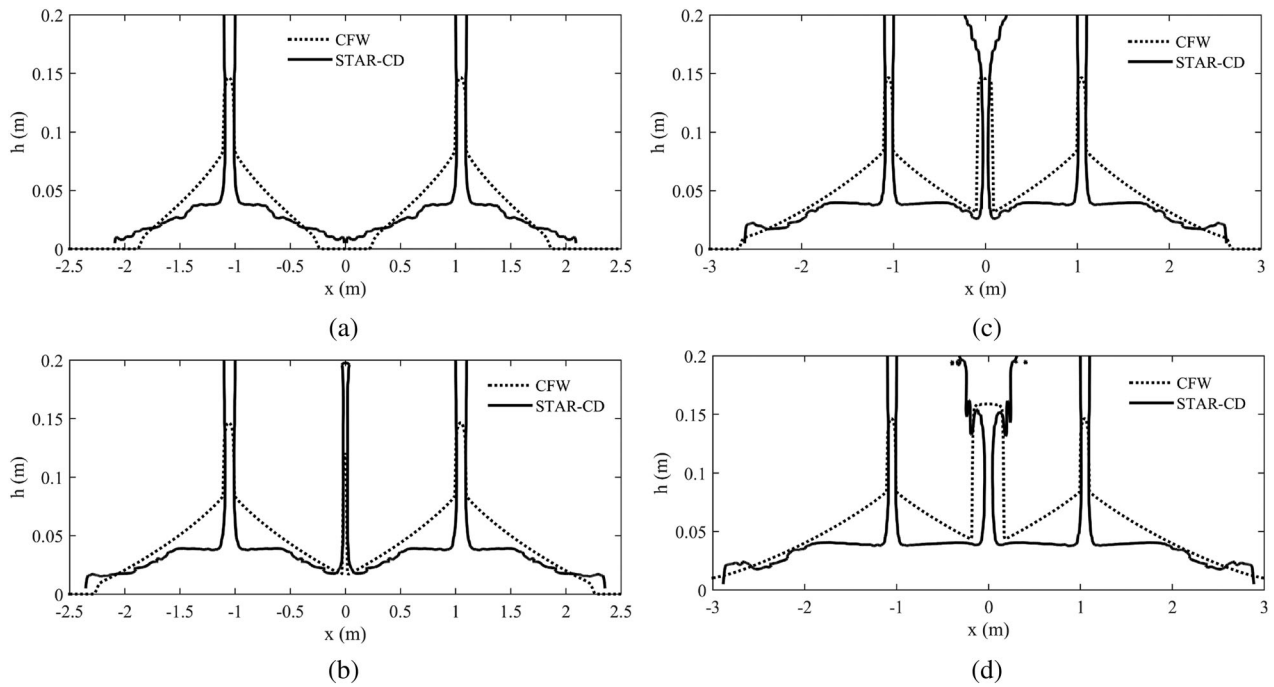
FIGURE 7 Comparison between the simulation results of the CFW and STAR-CD approaches in modelling sewer flow with two inflows for MN = 3.0294 at times t = 0.5, 0.7, 0.9 and 1.1 s (a–d). CFW, coupled flux wave; MN, manhole number.

TABLE 2 Error norm between the simulation results of SWE and NSE (STAR-CD) solvers in modelling sewerage with two inflows for MN = 2.0196.

Time (s)	l_∞	l_2
0.5	0.0182	4.6147×10^{-4}
0.7	0.1074	5.6967×10^{-4}
0.9	0.0495	3.1910×10^{-4}
1.1	0.0480	3.0223×10^{-4}

Abbreviations: MN, manhole number; NSE, Navier–Stokes equation; SWE, shallow water equation.

in the CFW method is considered as an efflux. Furthermore, the water height at collision point is different due to the increased speed raised from the gravitational falling in STAR-CD results. Table 2 shows the calculated error norm between the CFW solver and STAR-CD confirming that the relevant error is rather small. Based upon the three cases mentioned above with different velocity, it is considered in this case that the range of [2 3] for the MN gives the best performance of CFW approach. For the SWEs computations, 512 computational cells with $Cr = 0.5$ were used. In STAR-CD, a mesh with a step size of 0.01 m was considered, where in some locations, such as the collision points (from −0.5 to 0.5 m in x-direction and from 0 to 0.2 m in y-direction), the mesh was refined to half size. Moreover, the k-ε high-Reynolds number is utilised as a turbulence model in this case. The

total computational time for this test case using the CFW code was 0.72 s, whereas STAR-CD solver took 449.47 s.

Based on this test case (with a fixed geometry), if MN lies within 2 and 3, this suggests that the CFW model provides a good representation of the system has acceptable agreement exist between CFW and STAR-CD results even for the violent flow regimens where the pressure is dominated by non-hydrostatic distribution. In cases MN is outside the range, the difference between results may be higher and therefore, the compatibility decreases.

3.3 | Inflow caused by symmetric dam-break waves

The third test case investigates the inflow caused by two water volumes located on opposite sides of an open manhole inlet, 0.3 m in diameter and centred at 0 m (Figure 8). For the CFW solution, 256 cells and the Courant number of $Cr = 0.5$ were utilised. To examine the sensitivity of the findings to the choice of turbulence model, this case is conducted with the V2F model, to consider if this affects the agreement between the CFD and CFW approaches. The 'Pressure' boundary condition was considered for the top surface, and 'wall' condition was assigned to the sides of the manhole and top and bottom of the lower pipe. As can be seen from Figure 9, two masses of water collide with each other at around $t = 0.3$ s. Then, the water drops down from 50 cm height

FIGURE 8 Initial condition of inflow caused by dam-break waves.
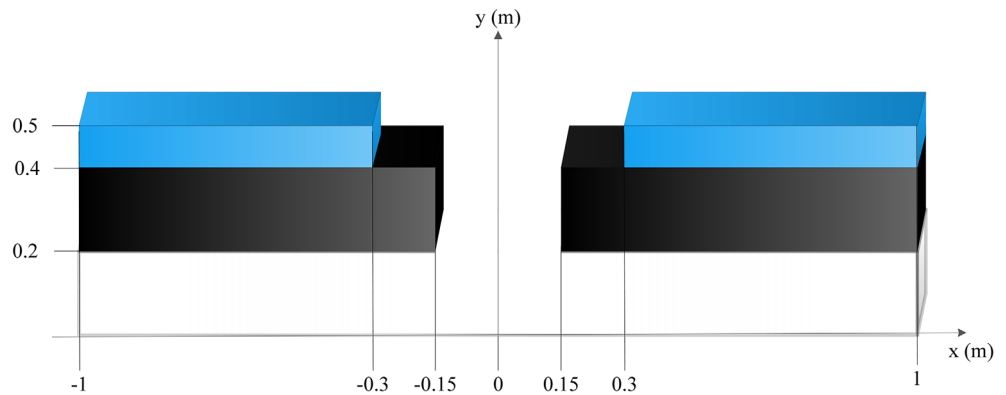
and reaches to zero level at $t = 0.51$ s, and consequently, propagates right- and left-wards within the underground pipe. Again, the CFW is not capable of modelling the drop; therefore, the volume of the dropping water is considered as a surcharged flow for the SWEs. As mentioned in Section 2, the surface overland and the underground flows are governed by second-order flux-wave approach to solving the SWEs. The water inside the manhole obeys the ODE proposed by Borsche and Klar (2014). The height and discharge provided by the ODE are imported into the CFW approach as inputs at each time step. Other than this difference, the agreement between CFW and STAR-CD results are very close for both overland and underground flows for all of the computed times. Table 3 presents the error norm calculated between the CFW and STAR-CD approaches. As can be seen, the maximum discrepancy for the results is at time $t = 0.61$ s, where the interacted manhole-shaft flows reach the bottom of the underground channel. As time passes, the differences between the error norms become smaller. Results suggest that the use of an alternate turbulence model, does not significantly affect the agreement between CFD and CFW approaches. The total computational time for this test case was 0.78 s for the CFW code and 13341.3 s for the STAR-CD solver.

3.4 | Comparison of CFW with experimental data

The main purpose of this test case is to assess the performance of the proposed numerical method against experimental data. Suitable data sets from a prior laboratory project focusing on surface/pipe flow interactions using a scaled physical model conducted at the University of Sheffield were made available. Results, open-access data sets and findings from this project have been previously published (e.g., Kitsikoudis et al., 2021; Rubinato et al., 2018); however, to date, the data sets have not been used to validate a fully integrated modelling approach able to

reproduce the time series evolution of surface depths around the interaction node during unsteady surcharge events. The experimental model facility was designed to study the interaction of overland/surface and piped drainage flow via a manhole. The surface channel is of length and width with longitudinal slope equal to 1/1000. A single vertical scaled manhole shaft connects the free-surface to an underground pipe system (no slope). The manhole centerline is located 2.095 m downstream of the fixed surface inflow weir. Inlet and outlet flow to the pipe system ($Q3$ and $Q4$) and inflow to the surface ($Q1$) are monitored by electromagnetic flow meters. In pipe Reynolds numbers were calculated to be >11,500 in all tested cases; hence, flow conditions were evaluated to be fully turbulent. The facility, relevant dimensions, instrumentation and complete set of open-access data from tests conducted in both steady and unsteady conditions are fully described in Rubinato et al. (2017).

The data used to validate the modelling approach described in this paper comprises of a single unsteady test case of 350-s duration from Rubinato et al. (2017) in which a fixed steady flow rate is passed over the weir at the upstream end of the surface flow channel ($Q1 = 8.23$ L/s), while an unsteady flow profile is reproduced in the pipe network using automated valves (Figure 10). At the beginning of the simulation, this results in net exchange of flow from the surface into the pipe network (influx/drainage case) with the manhole not completely full of water (i.e., free discharge conditions), as the flow rate in the pipe network is increased, the system transfers to an efflux/surcharge case (at $t \approx 100$) with a net transfer from the pipe network to the surface, before finally returning to a steady influx case (after $t \approx 160$). Pressure transducers (of type GEMS series 5000) were installed to measure flow depths throughout the simulation at various points on the surface downstream of the inflow weir. The measurement points used in this work are situated in line with the manhole centerline at points upstream and downstream of the manhole (Figure 11).
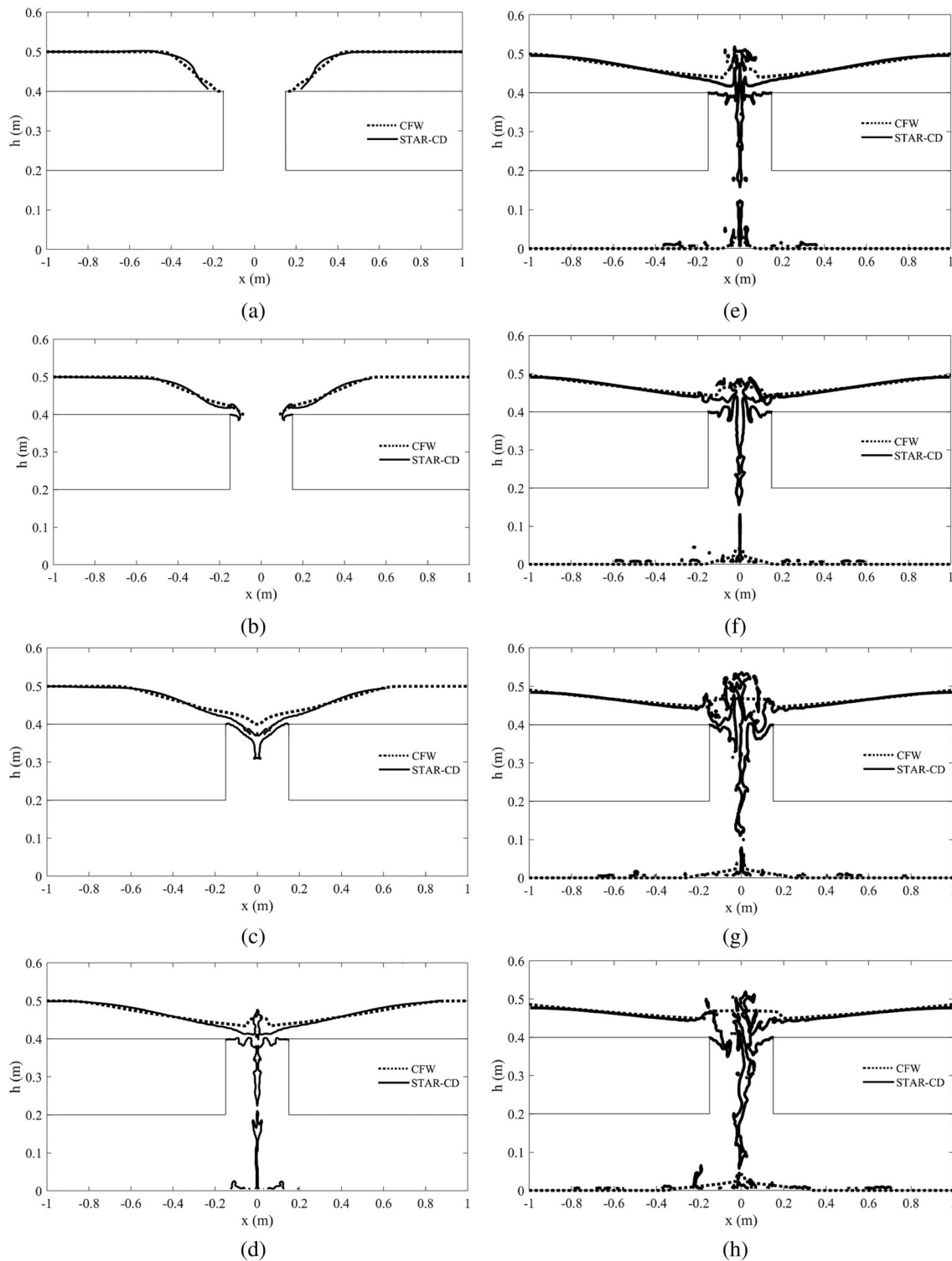
FIGURE 9 Comparison between the simulation results of the CFW and STAR-CD solver at $t = 0.1, 0.2, 0.3, 0.51, 0.61, 0.71, 0.81$ and 0.91 s (a–h) in modelling symmetric dam-break waves. CFW, coupled flux wave.

To compare the numerical results obtained based on the CFW approach, the appropriate measured flow conditions at the start of the simulation were imposed into the continuity equation of the SWEs provided in Equations (1a) and (1b). In terms of the boundary condition, the extrapolation boundary conditions (LeVeque, 2002), which resemble the open boundary for the wave propagation algorithm, have been employed.

Figure 12 illustrates the comparison between the numerical and the experimental measurements for

—WILEY

the free-surface flow at specific times $t = 20, 50, 70, 100, 120, 150, 170, 200, 250, 300$ and 350 s relative to the start of the simulation. Experimental values represent a temporal average over 2 s of data to reduce experimental variability. As can be seen until $t = 100$ s, the CFW results are very close to the experimental data. As the time

TABLE 3 Error norm between the simulation results of CFW and STAR-CD solvers in modelling the inflow caused by symmetric dam-break waves.

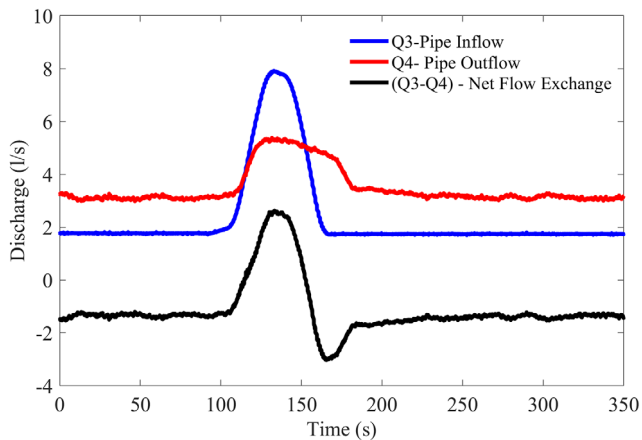| Time (s)	l_∞	l_2
0.1	0.0023	1.3161×10^{-5}
0.2	0.0014	1.1532×10^{-5}
0.3	0.0083	1.5214×10^{-5}
0.51	0.0111	1.8357×10^{-5}
0.61	0.0201	2.3423×10^{-5}
0.71	0.0187	2.1722×10^{-5}
0.81	0.0219	2.5912×10^{-5}
0.91	0.0216	2.5394×10^{-5}

Abbreviation: CFW, coupled flux wave.

FIGURE 10 Experimental data of inflow/outflow pipe discharges and net flow exchange over a period of 350 s (Q3 = Pipe Inflow, Q4 = Pipe Outflow, Q3–Q4 = Net exchange between surface and pipe systems).

increases (at $t = 100$ s and above), the system passes into surcharging state and the manhole efflux collides with the free-surface flow. This causes a small discrepancy between the CFW approach and the experimental data. The relevant error norms at the 8 measurement locations are calculated and presented in Table 4. Based upon the obtained error norm given in this table, the CFW results provide an excellent representation of the free-surface flow until surcharge occurs, after which some discrepancies are present close to the manhole and further downstream as the wave propagates over the surface.

Figure 13 shows the time series comparison between the pressure measurements achieved at the pressure transducers in the longitudinal direction (Figure 11) with the CFW code. As evident in this figure, the computed pressure data just upstream and downstream the manhole (P3 and P4) is in close agreement with the pressure measurement for the entire simulation. Differences are larger at measurement points further away from the manhole during the surcharge event. This might be because some waves dominated by non-hydrostatic pressure are created (in particular after $t = 100$ s) which cannot be accurately modelled using the SWEs. This discrepancy reduces after the fluid approaches steady conditions ($t \approx> 200$).

3.5 | Data analysis and discussion

The primary objective of this paper was to present a high-resolution FV solver that offers accuracy and the capability to simulate various complex unsteady interactions between pipe and surface flows through manholes. As shown in the previous sub-sections, The CFW solver proves to be computationally efficient compared to the 3D Navier–Stokes solver (simulation times with the CFW approach are 1.14, 0.72 and 0.78 s for dam-break interaction with two surcharging manholes, two manhole system, and inflow caused by symmetric dam-break waves, respectively. The simulations with the VOF solver last 1330.75, 449.47 and 13341.3 s, respectively, for the mentioned cases). The accuracy of the CFW approach was quantitatively analyzed by the
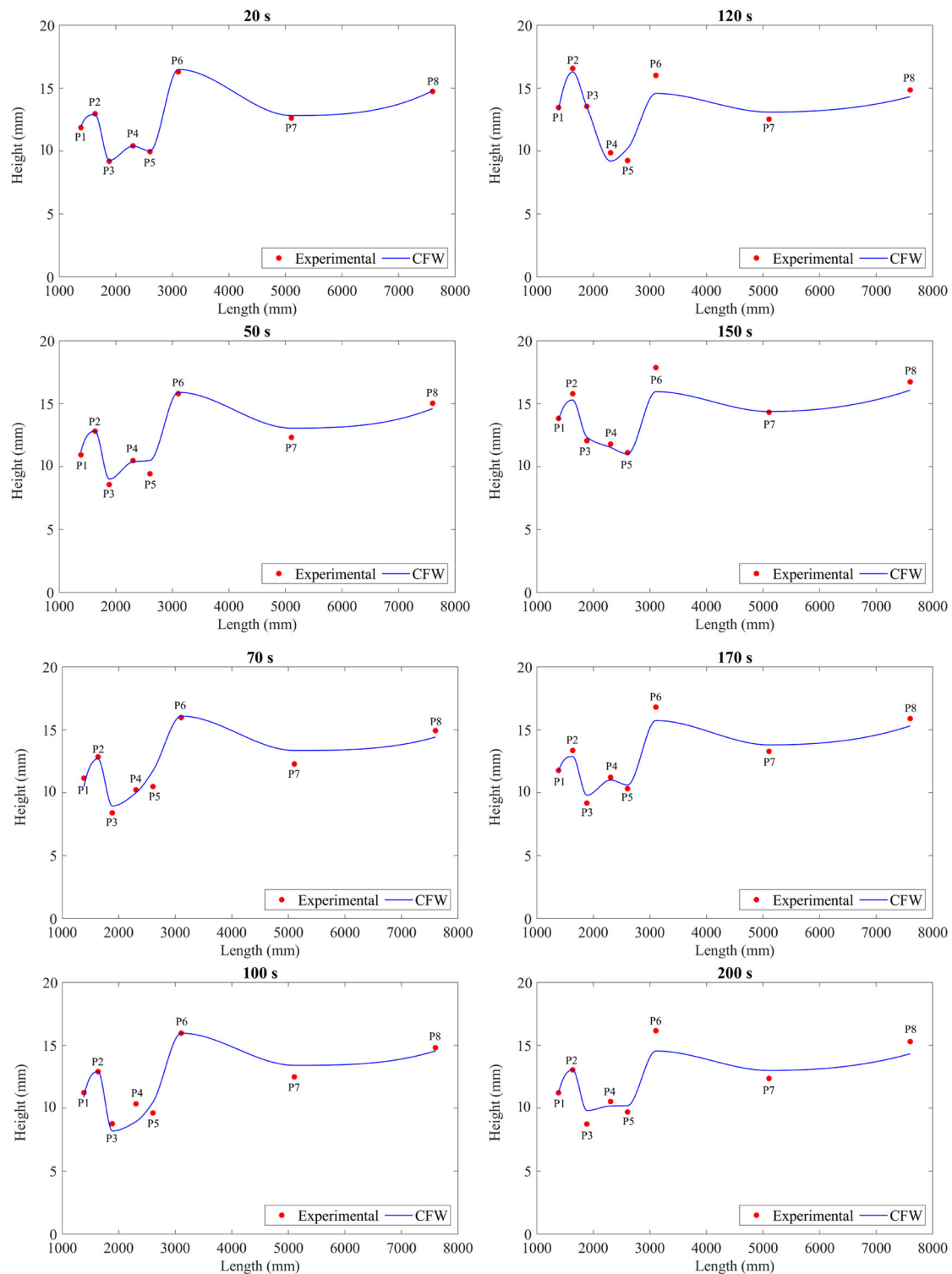

FIGURE 11 Position of flow depth measurement locations along the floodplain (distances are in mm, relative to the surface inflow weir). The manhole is positioned between measurement locations P3 and P4.

FIGURE 12 Experimental (measured) and CFW longitudinal water depth profile at times $t = 20, 50, 70, 100, 120, 150, 170, 200, 250, 300$ and 350 s.

calculation of the error norms. The values presented in Tables 1–4 of the calculated error norms lie within the range of 1.1532×10^{-4} m at the minimum and 3×10^{-3} m at the most critical stages when considering comparisons with both 3D numerical simulations and experimental observations. In these test cases, this represents mm scale differences in most spatial locations, which is negligible in terms of practical applications. Furthermore, it remains effective even in cases involving violent flow regimes characterised by non-hydrostatic pressure
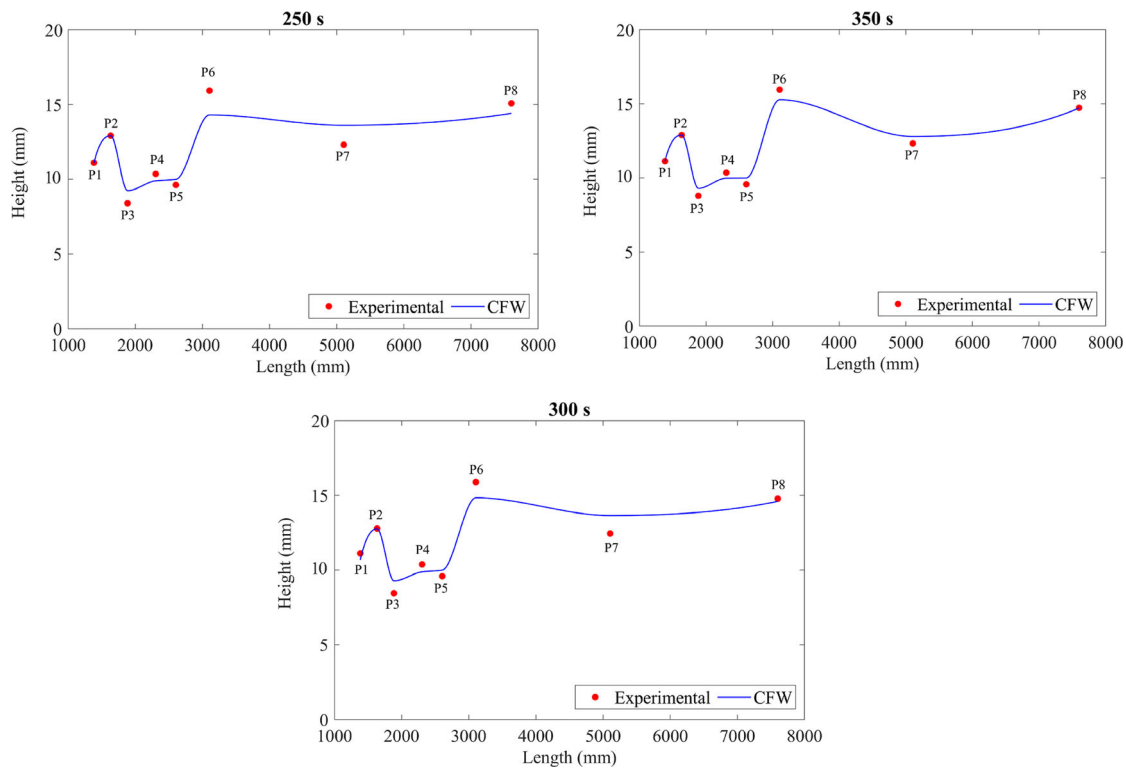
FIGURE 12 (Continued)

TABLE 4 Error norm between the simulation results of CFW and experimental data.

Time (s)	l_∞	l_2
20	0.002	4.0471×10^{-4}
50	0.0106	0.0018
70	0.0125	0.0024
100	0.0141	0.0025
120	0.0143	0.0025
150	0.0191	0.0027
170	0.0107	0.002
200	0.0161	0.0029
250	0.0162	0.0030
300	0.0121	0.0025
350	0.0068	0.0014

Abbreviation: CFW, coupled flux wave.

(see Section 3.3). These values demonstrate the accuracy and reliability of the CFW method despite the inherent limitations of the Eulerian approaches, specifically SWEs. The most important limitation of the CFW approach is the incapability of modelling free-fall conditions; for example, in Section 3.2, the flow in the VOF solver is injected from the top of the domain (0.2 m) into the manhole, while the

flow is considered as an efflux from the bottom of the domain in the CFW modelling. This results in some specific deviations between the CFW and STAR models in these cases (see Section 3.2). Additionally, other conditions may cause the uncertainties of the model, such as the limitations in turbulence models, and the near-wall treatment. Moreover, the CFW uses different formulations for the friction through the manhole (Borsche & Klar, 2014) and for the water propagating on the surface or in the sub-surface channels.

Overall, the CFW has demonstrated the capability to be employed without limitations in simulating surface flood problems integrated with a sewerage system. It should be noted that for practical reasons (computational cost, experimental data availability), the test cases explored here represent small/scaled systems when compared to practical drainage networks. Although flow conditions within test cases are fully turbulent (and thus any scaling errors are expected to be minor as energy loss mechanisms in full-scale systems are expected to be similar), it is recommended that further testing be conducted based on full-scale systems and larger drainage networks to give a better indication of performance for practical applications. In particular, further testing over a range of MNs should consider variations in network geometries as well as characteristic velocities.
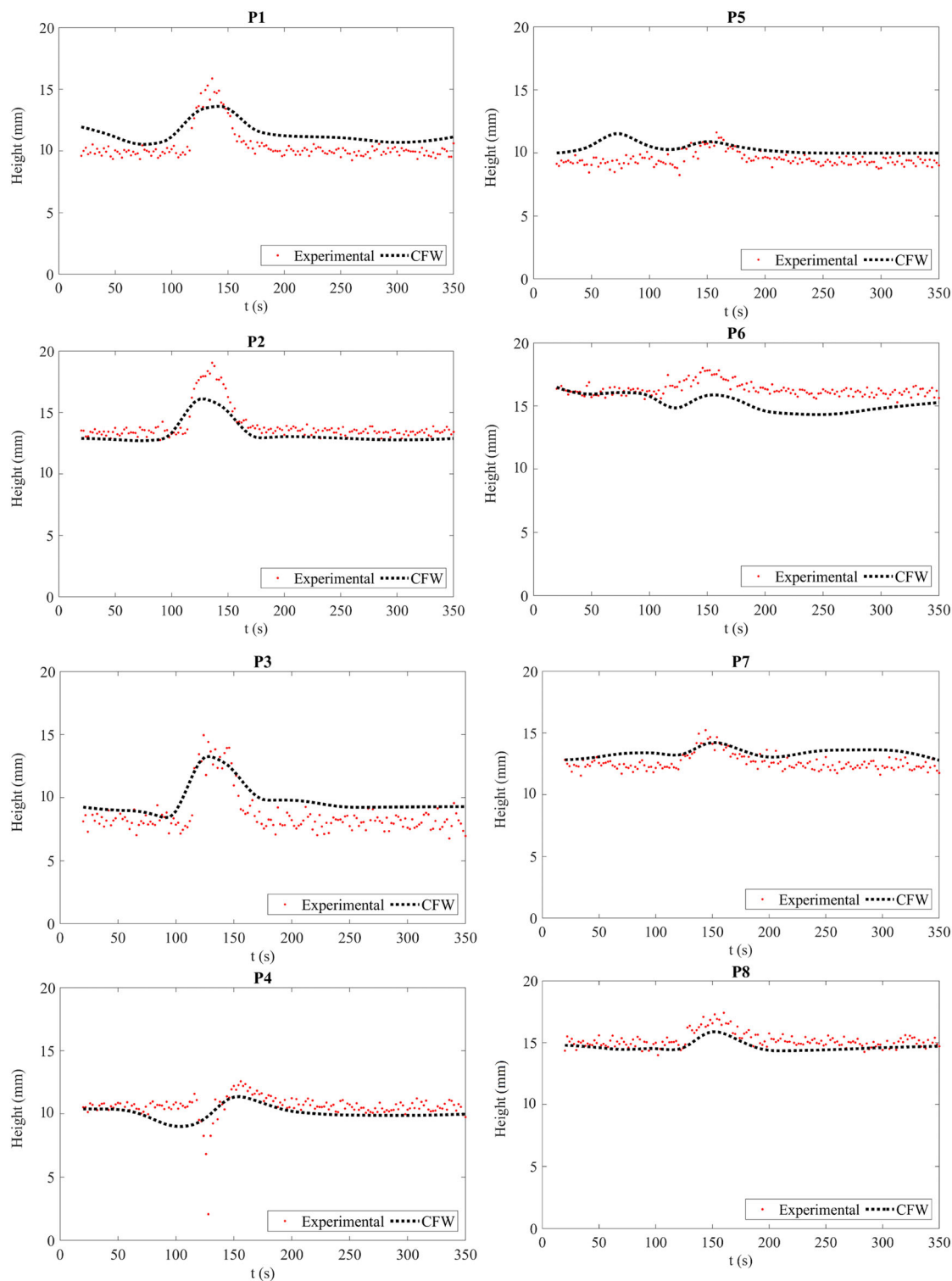
FIGURE 13 Time series comparison of experimental and CFW water levels at each measurement location.

4 | CONCLUSION

In this paper, a coupling approach, called the CFW method, was developed based on a modified version of the flux-wave formula, and utilised for modelling free-surface flood propagation over a dry bed and

surcharged flow in a sewer system. The numerical solver used here simulates 1D flooding situations for both free-surface flows as well as the manhole linking the overland to underground flow. The inflow/outflow discharges are treated within the continuity equation and therefore, the entire solution is preserved in

conservation laws form. To consider the effect of free-falling water in the CFW approach, the vertical discharge calculated by an ODE solver was added as a surcharged flow to the continuity equation in the SWEs. In addition to using the proposed SWEs solver, Navier–Stokes equations were solved for all cases using the STAR-CD software, and the results of the two methods were compared. Furthermore, the performance of the CFW approach was investigated against experimental data. The experimental set-up built at the University of Sheffield was designed to study the interaction of overland and piped drainage flow via a manhole, and time-varying flow depths under unsteady manhole surcharge conditions are presented here for the first time.

The major novel contribution of this work is the validation of a modelling approach which considers total energy and momentum exchange between pipe and surface flows and is practically applicable for simulating drainage networks. As such, the main potential application is the consideration of highly unsteady flood flows within urban flood cases, in which the consideration of surface waves within linked surface/sub-surface flow systems is of value to the model user.

DATA AVAILABILITY STATEMENT
Open access data sets associated with this project can be found at https://zenodo.org/communities/floodinteract/.

ORCID
Sadegh Moodi https://orcid.org/0000-0002-5138-2956
Hossein Mahdizadeh https://orcid.org/0000-0002-1056-7583
James Shucksmith https://orcid.org/0000-0001-5497-0051

REFERENCES
Bale, D. S., Leveque, R. J., Mitran, S., & Rossmanith, J. A. (2003). A wave propagation method for conservation laws and balance laws with spatially varying flux functions. *SIAM Journal on Scientific Computing*, 24(3), 955–978.
Beg, M. N. A., Rubinato, M., Carvalho, R. F., & Shucksmith, J. D. (2020). CFD modelling of the transport of soluble pollutants from sewer networks to surface flows during urban flood events. *Water*, 12(9), 2514.
Borsche, R., & Klar, A. (2014). Flooding in urban drainage systems: Coupling hyperbolic conservation laws for sewer systems and surface flow. *International Journal for Numerical Methods in Fluids*, 76(11), 789–810.
de Vitry, M. M., & Leitão, J. P. (2020). The potential of proxy water level measurements for calibrating urban pluvial flood models. *Water Research*, 175, 115669.
Djordjević, S., Prodanović, D., Maksimović, Č., Ivetić, M., & Savić, D. (2005). SIPSON–simulation of interaction between pipe flow and surface overland flow in networks. *Water Science and Technology*, 52(5), 275–283.
Dong, B., Xia, J., Zhou, M., Deng, S., Ahmadian, R., & Falconer, R. A. (2021). Experimental and numerical model studies on flash flood inundation processes over a typical urban street. *Advances in Water Resources*, 147, 103824.
El Kadi Abderrezzak, K., Paquier, A., & Mignot, E. (2009). Modelling flash flood propagation in urban areas using a two-dimensional numerical model. *Natural Hazards*, 50(3), 433–460.
Fraga, I., Cea, L., & Puertas, J. (2017). Validation of a 1D-2D dual drainage model under unsteady part-full and surcharged sewer conditions. *Urban Water Journal*, 14(1), 74–84.
George, D. L. (2008). Augmented Riemann solvers for the shallow water equations over variable topography with steady states and inundation. *Journal of Computational Physics*, 227(6), 3089–3113.
Gómez, M., Russo, B., & Tellez-Alvarez, J. (2019). Experimental investigation to estimate the discharge coefficient of a grate inlet under surcharge conditions. *Urban Water Journal*, 16(2), 85–91.
Gosman, A. (1969). *Heat and mass transfer in recirculating flows*. Academic Press.
Hong, S. W., & Kim, C. (2011). A new finite volume method on junction coupling and boundary treatment for flow network system analyses. *International Journal for Numerical Methods in Fluids*, 65(6), 707–742.
Issa, R., Ahmadi-Befrui, B., Beshay, K., & Gosman, A. (1991). Solution of the implicitly discretised reacting flow equations by operator-splitting. *Journal of Computational Physics*, 93(2), 388–410.
Issa, R. I. (1986). Solution of the implicitly discretised fluid flow equations by operator-splitting. *Journal of Computational Physics*, 62(1), 40–65.
Kitsikoudis, V., Erpicum, S., Rubinato, M., Shucksmith, J. D., Archambeau, P., Pirotton, M., & Dewals, B. (2021). Exchange between drainage systems and surface flows during urban flooding: Quasi-steady and dynamic modelling in unsteady flow conditions. *Journal of Hydrology*, 602, 126628.
Leandro, J., Chen, A. S., Djordjević, S., & Savić, D. A. (2009). Comparison of 1D/1D and 1D/2D coupled (sewer/surface) hydraulic models for urban flood simulation. *Journal of Hydraulic Engineering*, 135(6), 495–504.
Leandro, J., & Martins, R. (2016). A methodology for linking 2D overland flow models with the sewer network model SWMM 5.1 based on dynamic link libraries. *Water Science and Technology*, 73(12), 3017–3026.
Lee, S., & An, H. (2019). Evaluating the effect of grid size and type in integrated 1D/2D coupled urban inundation modelling on the interacting discharge between the surface and sewerage system. *Journal of Flood Risk Management*, 12, e12537.
LeVeque, R. J. (1998). Balancing source terms and flux gradients in high-resolution Godunov methods: The quasi-steady wave-propagation algorithm. *Journal of Computational Physics*, 146(1), 346–365.

LeVeque, R. J. (2002). *Finite volume methods for hyperbolic problems* (Vol. 31). Cambridge University Press.

Lopes, P., Leandro, J., Carvalho, R. F., Páscoa, P., & Martins, R. (2015). Numerical and experimental investigation of a gully under surcharge conditions. *Urban Water Journal*, *12*(6), 468–476.

Mahdizadeh, H., & Sharifi, S. (2019). A fully-coupled bedload sediment transport model based on a two-dimensional modified wave propagation algorithm. *Journal of Hydraulic Research*, *58*(2), 187–203.

Mahdizadeh, H., Sharifi, S., & Omidvar, P. (2018). On the approximation of two-dimensional transient pipe flow using a modified wave propagation algorithm. *Journal of Fluids Engineering*, *140*(7), 071402.

Mahdizadeh, H., Stansby, P. K., & Rogers, B. D. (2011). On the approximation of local efflux/influx bed discharge in the shallow water equations based on a wave propagation algorithm. *International Journal for Numerical Methods in Fluids*, *66*(10), 1295–1314.

Mahdizadeh, H., Stansby, P. K., & Rogers, B. D. (2012). Flood wave modeling based on a two-dimensional modified wave propagation algorithm coupled to a full-pipe network solver. *Journal of Hydraulic Engineering*, *138*(3), 247–259.

Martínez, C., Vojinovic, Z., Price, R., & Sanchez, A. (2021). Modelling infiltration process, overland flow and sewer system interactions for urban flood mitigation. *Water*, *13*(15), 2028. https://www.mdpi.com/2073-4441/13/15/2028

Martins, R., Kesserwani, G., Rubinato, M., Lee, S., Leandro, J., Djordjević, S., & Shucksmith, J. (2017). Validation of 2D shock capturing flood models around a surcharging manhole. *Urban Water Journal*, *14*(9), 892–899.

Martins, R., Leandro, J., & Djordjević, S. (2018). Influence of sewer network models on urban flood damage assessment based on coupled 1D/2D models. *Journal of Flood Risk Management*, *11*, S717–S728.

Patankar, S. (1980). *Numerical heat transfer and fluid flow, hemisphere*, Washington DC. Publishing Corporation.

Patankar, S. V., & Spalding, D. B. (1972). A calculation procedure for heat, mass and momentum transfer in three-dimensional parabolic flows. *International Journal of Heat and Mass Transfer*, *15*(10), 1787–1806.

Rodi, W. (1979). Influence of buoyancy and rotation on equations for the turbulent length scale. In *2nd symposium on turbulent shear flows*.

Rubinato, M., Lashford, C., & Goerke, M. (2021). Advances in experimental modelling of urban flooding. In X. C. Wang & G. Fu (Eds.), *Water-wise cities and sustainable water systems: Concepts, technologies, and applications*. IWA Publishing. https://doi.org/10.2166/9781789060768_0235

Rubinato, M., Martins, R., Kesserwani, G., Leandro, J., Djordjević, S., & Shucksmith, J. (2017). Experimental calibration and validation of sewer/surface flow exchange equations in steady and unsteady flow conditions. *Journal of Hydrology*, *552*, 421–432.

Rubinato, M., Martins, R., & Shucksmith, J. (2018). Quantification of energy losses at a surcharging manhole. *Urban Water Journal*, *15*(3), 234–241.

Schmidt, D. P., Rutland, C. J., & Corradini, M. (1997). A numerical study of cavitating flow through various nozzle shapes. *SAE Transactions*, *106*, 1664–1673.

Tahry, S. H. E. (1983). K-epsilon equation for compressible reciprocating engine flows. *Journal of Energy*, *7*(4), 345–353.